A Cardiac Transcriptional Enhancer is Repurposed During Regeneration to Activate an Anti-proliferative Program.

Anupama Rao[1], Andrew Russell[1#], Jose Segura-Bermudez[1#], Charles Franz[1#], Anton Blatnik[1], Jacob Panten[2], Mateo Zevallos[1], Maciej Pietrzak[3] and Joseph Aaron Goldman[1*]

[1]Department of Biological Chemistry and Pharmacology, The Ohio State University Medical Center, Columbus OH

[2]Department of Molecular Genetics, The Ohio State University, Columbus OH

[3] Department of Biomedical Informatics, The Ohio State University, Columbus OH

[#]these authors contributed equally

*corresponding author (aaron.goldman@osumc.edu)

1060 Carmack Rd
Rightmire Hall 105
Columbus, OH 43210
857-600-6488

Abstract:
Zebrafish have a high capacity to regenerate their hearts. Several recent studies have surveyed transcriptional enhancers to understand how the dynamics of gene expression are controlled during regeneration. Here, we describe an enhancer, called *REN*, that controls expression around cardiac valves in uninjured hearts and is then repurposed for activating transcription in regenerating tissue. Interestingly, REN activity around valves is perfectly anti-correlated with the site of injury. Although, *REN* has the hallmarks of activating a pro-regenerative program, deletion mutants have increased CM proliferation suggesting *REN* activates an anti-proliferative program. We show that *REN* is an essential enhancer for *runx1,* a nearby gene that when mutated has similar increases in CM proliferation. *REN* mutants lack appreciable differences in cardiac scar formation, eliminating this *runx1* specific phenotype as a cause for the increased CM proliferation. Thus, the enhancer mutants revealed a more detailed model of *runx1* function than what could be appreciated from the gene mutant alone. *REN* deletion mutants also had phenotypes in uninjured hearts, that we show is independent of *runx1*. Our data point to a new mechanism for gene control during zebrafish heart regeneration where an enhancer from one cardiac domain is repurposed to activate a different nearby gene at the site of regeneration.

Introduction

Zebrafish have a profound ability to regenerate damaged heart muscle. Heart regeneration proceeds via the proliferation of pre-existing cardiomyocytes (CMs) that replace myocardium lost to injury(Jopling et al., 2010; Kikuchi et al., 2010). Thousands of genes change expression levels in a coordinated, injury-responsive program that leads to CM proliferation and other key cell behaviors. Several groups have identified tissue regeneration enhancer elements (TREEs) in zebrafish, regulatory sequences that activate gene expression in different cell types within the regenerating heart and in other organs in response to injury and during regeneration (Cao et al., 2022; Goldman et al., 2017; Kang et al., 2016; Lee et al., 2020; Sun et al., 2022; Thompson et al., 2020). Interestingly, attempts to demonstrate *in vivo* requirements for an enhancer by deletion has seldom led to a resultant regeneration phenotype (Sun et al., 2022; Wang et al., 2020). In killifish, deletion of an enhancer upstream from *inhibin beta* resulted in impaired heart regeneration and suggested a model for how evolutionary changes in enhancer elements develop together with regeneration capacity (Wang et al., 2020). A second deletion of an enhancer upstream of *cebpd* led to impaired epicardial proliferation and phenotypes in the brain where the enhancer is also activated during regeneration (Sun et al., 2022). However, most enhancers are validated using transgenic reporters that just reveals expression domains and dynamics but do not reveal mechanistic activities at the core of how endogenous enhancers are recruited during regeneration.

Regeneration phenotypes are likely difficult to recover because genes are rarely dependent on a single enhancer and multiple enhancers increase the possibility of functional redundancy (Bolt and Duboule, 2020; Kvon et al., 2021). During zebrafish development, Hi-C chromosome capture sequencing uncovered an average of 4.85 enhancers per gene and 2.6 genes linked to a single enhancer (Yang et al., 2020). Multiple enhancers often coordinate upon a single gene (Fulco et al., 2016; Panigrahi and O'Malley, 2021) and push the equilibrium towards phase separation and gene activation (Hnisz et al., 2017; Sabari et al., 2018). However, mechanisms explaining the reverse or how a single enhancer regulates multiple genes are somewhat more elusive. Single enhancers have been reported to interact with multiple promoters in "hubs" of several coregulated genes (Uyehara and Apostolou, 2023) that are often responsible for similar developmental processes (Abascal et al., 2020; Fanucchi et al., 2013; Miguel-Escalada et al., 2019; Pelham-Webb et al., 2020). Other experimental models have suggested that multiple promoters may compete for enhancer activation often at the mutual expense of their expression (Cho et al., 2018; Dao et al., 2017; Fukaya et al., 2016; Lim et al., 2018; Oudelaar et al., 2019). Both the models of enhancer hubs and promoter competition where a single enhancer regulates multiple genes reflect situations when coregulation of the shared genes is important. Instances of actual 're-wiring' of enhancer connectomes to different genes has been observed in cancers, resulting in misactivation of oncogenes, or in developmental contexts when insulator deletion leads to enhancer communication with genes in different neighborhoods (Lupiáñez et al., 2015; Melo et al., 2020; Nameki et al., 2023; Okada and Saga, 2022; Youngblood et al., 2023). Examples of regulated switching of an enhancer between two genes are also described for locus control regions that govern developmental switching particularly between embryo and adult (Wilber et al., 2011). How dynamics between enhancers and promoters are governed during regeneration are not well described.

Previously, we produced an atlas of nucleosome turnover in the zebrafish heart to identify regeneration specific genes and regulatory elements (Goldman et al., 2017). Using a transgenic histone H3.3, we profiled changes in chromatin accessibility in CMs. Dozens of loci containing enrichment of H3.3 were validated in transgenic reporter assays as enhancers, some of which were exclusive to CMs and others that also stimulated reporter expression in other cell-types. One such reporter contained a 1265bp region found 103kb upstream from the *runx1* locus with H3.3 enrichment that increased during heart regeneration. This *runx1*-linked enhancer (or REN) activated GFP in proliferating cells within the

wound of a regenerating heart. REN was not just injury responsive but was also activated in proliferating CMs in a transgenic model of CM hyperplasia where the Nrg1 protein stimulates proliferation rather than injury (Goldman et al., 2017). Thus, H3.3 profiling in regenerating hearts identified a genetic marker for proliferating CMs. However, what this enhancer regulates and its importance to regeneration remain unknown.

Here, we demonstrate how the role of REN unexpectedly changes from uninjured hearts to regeneration. REN stimulates gene expression in a subdomain of cardiac tissue that surrounds valves leading to the outflow track of the heart. During regeneration, activity around the valve is inversely correlated with REN stimulation in regenerating tissue. REN activity peaks just before and during the peak of regeneration, and in models of CM hyperplasia, suggests that REN functions to activate a pro-regenerative gene expression program. Surprisingly, zebrafish mutants with REN deleted have *improved* proliferation of CMs after injury suggesting REN controls an anti-proliferative program which is linked to control of *runx1* expression in a subset of cell-types. REN deletion mutants also have phenotypes around valves in uninjured hearts that are independent of *runx1*. Taken together, this suggests that REN is an enhancer that is repurposed from one cardiac domain to stimulate gene expression in regenerating tissue.

The REN enhancer directs gene expression in cardiac muscle and epicardium.

Previously, we showed that a transgenic reporter containing the REN enhancer cloned upstream of a minimal promoter was able to activate GFP in proliferating cells during heart regeneration(Goldman et al., 2017). REN was first identified using a CM-specific profiling method which is consistent with *REN:GFP* expression co-staining with an antibody targeting the myosin heavy chain in heart muscle 7days-post-amputation (dpa) (Fig. 1A). However, we also observe a significant amount of GFP that is not in the muscle from other cardiac cell-types (Fig. 1B). The epicardium, a cell layer enveloping the heart, and endocardium, a second single-cell layer covering the heart lumen are important tissues required for signaling to the myocardium during regeneration (Kikuchi and Poss, 2012; Kikuchi et al., 2011a; Lowe et al., 2019; Lowe et al., 2021; Wang et al., 2015). To determine whether *REN:GFP* expression also occurs in the epicardium we injured fish containing both *REN:GFP* and *tcf21:mCherry* reporter transgenes and found extensive colocalization in every injured heart (Fig. 1CD) (Kikuchi et al., 2011b). Similarly, we tested *REN:GFP* and *flk1:mCherry* double reporter fish for *REN* directed expression in endocardium (Wang et al., 2010). *REN:GFP* activates in a few isolated endocardial cells and not in every heart (Fig. 1E). Only a few isolated *REN:GFP* and *flk:mCherry* colocalized cells are detected within the injury area representing less than 1% of the total *flk*-positive cells (Fig. 1F, mean 3dpa = 2.0, mean 7dpa = 2.3; N=9,10). We conclude that REN is a regulatory element with predominantly myocardial and epicardial enhancer activity during heart regeneration.

Activation of epicardium (1-3dpa) precedes the peak of CM proliferation (7dpa) during zebrafish heart regeneration (Kikuchi and Poss, 2012). To determine the temporal regulation of REN driven expression we performed a time course on *REN:GFP* reporter fish. The peak of total *REN:GFP* expression occurs at 3dpa coinciding with activated epicardium throughout the heart (Fig. S1A), and is slightly decreased at 7dpa plateauing by 14-30dpa (Fig. S1B). Increased expression of GFP at 3dpa likely reflects a broader distribution of *REN:GFP* positive cells. To measure the potency of transcriptional stimulation we calculated average fluorescence intensity of GFP in colocalized cells. *REN:GFP* intensity did not change in *tcf21:mCherry* cells that colocalized with *REN:GFP* between 3 and 7dpa despite the fact that there were fewer cells at 7dpa (Fig. 1G, magenta dots, 3dpa: tcf21+GFP average = 20,395 Arbitrary Density Units(ADU)/pixel^2; 7dpa: tcf21+GFP average = 24,269 ADU/pixel^2; Welch's t-test, $p = 0.4481$). Nor is there any change in average fluorescence intensity in CMs that colocalized with *REN:GFP* (Fig. 1G, blue dots, 3dpa:MHC+GFP average = 2770 ADU/pixel^2, 7dpa:MHC+GFP average = 2515 ADU/pixel^2, Mann-Whitney test, $p > 0.9999$). At 3dpa there is 7.36-fold more GFP intensity in epicardial cells versus CMs and 9.65-fold more GFP intensity at 7dpa, suggesting REN has more potent activity in the epicardium (Fig. 1G, 3dpa: Mann-Whitney $p < 0.0001$ N = 15,14, 7dpa: Mann-Whitney $p < 0.0001$, N=10,10). However, we cannot exclude that cell-specific qualities such as size or shape may influence differences in how GFP is localized impacting the observed intensity difference. We conclude that REN:GFP peaks throughout the heart at 3dpa, is focused at the site of injury by 7dpa, and is brighter in the epicardium than the myocardium.

Minimal components of REN contain binding motifs for known pro-regeneration transcription factors.

To identify the minimal sequence components that promote REN activity we produced new transgenic reporter lines with sub-fragments of REN cloned upstream of a minimal promoter driving GFP. Previously, we found DNA sequence motifs enriched in regeneration specific H3.3 peaks and ranked them by their specificity to regeneration(Goldman et al., 2017). Using the FIMO analysis tool we searched the REN enhancer for enrichment of these Cardiac Regeneration Motifs (or CRMs) and found four clusters of CRMs that included some of the most regeneration specific sequences (Fig. S2A)(Cuellar-Partida et al., 2012). Using the four clusters of CRMs as a guide, we divided REN into four blocks and made transgenic reporters containing these blocks in different combinations (Fig. 2A).

To define a minimal fragment responsible for REN epicardial expression we looked for fragments of REN that retained expression in epicardium. A fragment containing an extended region encompassing the first two blocks, called REN-b12+ is sufficient for activating GFP in *tcf21* positive cells (Fig. 2B). A second fragment containing just the blocks 1 and 2 called REN-b12 is not able to activate in the epicardium (Fig. 2C) nor is the smaller REN-b1x fragment (Fig. 2D). Therefore, the 375bp extended region of REN-b12+ beyond blocks 1 and 2 is necessary for epicardial activity. However, a transgenic reporter containing block 2 and the 375bp extended region (b2+) does not activate GFP at all during regeneration. This suggests that the 375bp region is necessary but not sufficient for epicardial GFP activation.

Amputation of the ventricle apex is a standard injury model that is sufficient for full-length REN activity. However, it is possible that more severe injury models would uncover GFP activity from the sub-fragments of REN that do not activate after amputation. Therefore, we crossed our REN fragments into the zebrafish cardiac ablation transgenic system (ZCAT) where CM-specific Cre releases the diphtheria toxin stochastically throughout the heart resulting in ablation of up to 60% of CMs (Wang et al., 2011). Most of the REN subfragments that are silent by amputation remain silent during genetic ablation (REN-b34, REN-b2, REN-b2+, Fig. S2B-D). The one fragment that does activate GFP, REN-deuce27, does so in non-CM cells within the heart wall (Fig. S2E). The ZCAT transgenic ablation system includes a red transgenic marker so we could not confirm whether these cells are epicardial using our *tcf21* reporter. However, the expression pattern is highly reminiscent of epicardium raising the possibility that the region responsible for REN expression in epicardium is a 140bp fragment that overlaps with REN-deuce27 and REN-b12+. Further investigation will be required to confirm whether this 140bp region directs epicardial expression from REN.

The minimal fragment required for CM expression from REN was more straightforward. The three transgenic fragments containing block 1 can drive GFP in CMs at 7dpa (Fig. 2E-H). Any fragment of REN that does not have block 1 also does not activate GFP in CMs (Fig. S2B-D). The most regeneration specific motif within block 1, CRM17, has homology to binding sites of the AP1 transcription factor complex (JASPAR, p = .0175) previously reported to be required for CM proliferation (Beisaw et al., 2020). Therefore, we isolated a 267bp minimal fragment of REN that is both necessary and sufficient for *REN* myocardial activity during regeneration and that contains binding sites for known regulators of CM proliferation.

REN regulates _runx1_ expression in a subset of cardiac cell-types during regeneration.

Multiple lines of evidence suggest that REN promotes a pro-regenerative gene expression program. First, REN directs expression in proliferating CMs independent from injury (Goldman et al., 2017). Second, REN activity peaks just before and during the peak of CM proliferation during regeneration (Fig. 1). Finally, a minimal fragment of REN that retains activity in CMs also harbors binding sites for transcription factors already shown to be required for regeneration (Fig. 2). To address whether REN is part of a pro-regeneration gene regulatory network, we stably deleted a 3,162bp region of the genome encompassing *REN* using CRISPR that we call Δ*REN* (Fig. S3A). Then we tested Δ*REN* mutants for their ability to complete regeneration. Based on the evidence from the reporter, we hypothesize that homozygous mutants lacking the *REN* enhancer would have impaired regeneration. We performed surgeries where we amputated the apex of Δ*REN* mutants and their wildtype siblings and looked if regeneration was completed by 30 days. Surprisingly, the Δ*REN* mutants have complete regrowth of cardiac muscle and nearly complete absence of scar indistinguishable from their wildtype siblings (Fig. 3AB). We conclude that REN is not necessary to complete regeneration.

To examine the possibility that Δ*REN* mutants have delayed regeneration times or more subtle defects, we measured CM proliferation levels at an earlier time point in Δ*REN* mutants and their wildtype clutch mates. We co-stained hearts recovering from amputation of the ventricle apex with

Mef2, a marker for CM nuclei, and EdU, a marker of cell cycling (Fig. 3C). Unexpectedly, we find that Δ*REN* mutants have a significant *increase* in CM cycling compared to wildtype clutch mates (Fig. 3D). The fraction of Mef2 positive CMs that are also positive with the proliferation marker EdU is increased by 28.5% at 7dpa (Fig. 3D, mean: wildtype = 9.11% and mutant = 11.71%, p-value = 0.0094, N = 24 vs 19). There is no difference in CM cycling levels between Δ*REN* mutants and wildtype siblings in uninjured hearts (Fig. S3B). Also, there is no increase in overall CM numbers in adult Δ*REN* mutant hearts compared to their wildtype siblings (Fig. S3C). Thus, we conclude that Δ*REN* mutants have increased levels of CM proliferation that are specific to heart regeneration. This is in stark contrast to our expectations and suggest that REN is inducing expression of an anti-proliferative program.

Since *REN* is a transcriptional enhancer, we expected that its deletion would cause gene expression changes during regeneration. RNAseq of Δ*REN* mutant hearts and their wildtype siblings during regeneration show transcripts that were relatively increasing or decreasing in Δ*REN* mutants. We performed linear regression analysis on the 2,036 transcripts changing during regeneration in wildtype hearts and the 2,159 transcripts changing during regeneration in the mutant and find 305 transcripts where the fold-change during regeneration was different (Fig. 3E). There are 141 transcripts where the fold-change is relatively decreased in Δ*REN* mutants (Fig. 3E, blue dots) and another 164 transcripts where the fold-change is relatively increased in the Δ*REN* mutants (Fig. 3E, red dots). We conclude that deletion of *REN* results in dysregulation of gene expression during heart regeneration.

To identify cell-type specific expression of the differential genes we looked for enrichment of CM-specific H3.3 at their promoters (Goldman et al., 2017). Of the 305 transcripts with differential fold-change, 187 had the CM-specific H3.3 in their promoters during regeneration suggesting that the genes are expressed in CMs (Fig. 3F). The promoters of another 23 genes expressing transcripts whose levels change in Δ*REN* mutants have active chromatin marks (H3K27ac) but not H3.3-CM (Goldman et al., 2017) suggesting expression in other cell-types besides CMs. Taken together, 61% of transcripts disrupted in Δ*REN* mutant hearts are expressed in CMs with only 7.5% specific to other cell-types. We cannot exclude that H3.3 positive genes are being expressed in other cells *in addition* to muscle but do conclude that upon deletion of REN, most dysregulated genes occur in CMs.

Several of the 50 transcripts that increase during regeneration in Δ*REN* mutants are known regulators of cardiac regeneration. For example, in mice epicardial expression of Fstl1 increases CM proliferation and in Δ*REN* mutants *fstl1a* mRNA is 4X more abundant during regeneration (increased 22.14–fold in Δ*REN* mutants, increased 5.48-fold in wildtype)(Wei et al., 2015). Also, *fibronectin 1a* (*fn1a*) is required for zebrafish heart regeneration and *fn1a* transcripts increases 11.57–fold in Δ*REN* mutants, but only 6.12–fold in wildtype siblings (Wang et al., 2013). Expression of *ankdr1a*, also known as CARP, increases 52.82-fold in Δ*REN* mutants but only 12.96-fold in wildtype regeneration. An enhancer for CARP called *2ankrd1aEN* was found together with *REN* using H3.3 profiling and *2ankrd1aEN* can drive gene expression at the site of injury in both mouse and porcine hearts (Yan et al., 2022). For example, *anln* which encodes a protein required for cytokinesis (increased 6.19–fold in Δ*REN* mutants, increased 2.41–fold in wildtype, residual = 1.72)(Oegema et al., 2000; Takayama et al., 2003). The increased induction of pro-regeneration and pro-proliferation genes in Δ*REN* mutants supports our observation of improved proliferation of CMs (Fig. 3D).

Based on the expression of the reporter transgenic line, genes that are a direct target(s) of REN would be expected to *decrease* in abundance when *REN* is deleted. There were 103 transcripts that decreased relatively in mutant hearts during regeneration (Fig. 3E, red dots, Table 1). Only three of these transcripts are encoded in genes on chromosome 1 with REN; however, it is unlikely that they are direct targets. For example, *meis1* is transcription factor involved in maturation of CMs (Mahmoud et al., 2013), that increases 5.67-fold in wildtype regeneration but doesn't increase in Δ*REN* mutants. However, the *meis1* gene is 49.97Mbp away from REN on the other end of the chromosome.

Enhancers have been reported to interact with promoters at incredible distances including between different chromosomes (Markenscoff-Papadimitriou et al., 2014), although by chromosome capture, promoters and enhancers interact within 1Mb ~80% of the time (Rao et al., 2014). From experimentally validated enhancer-gene associations, the largest reported distance between an enhancer and its cis-regulated promoter is 1.7Mb away for the Myc gene in mouse (Bahr et al., 2018; Gasperini et al., 2019). We find it unlikely that the three genes downregulated on chromosome 1 in REN mutants are being regulated from 25-50 Mbp away and conclude that the direct target of *REN* was not identified by RNAseq.

Published experiments using Hi-C have detailed topologically associating domains (TADs) of self-associating chromatin from adult zebrafish brain and skeletal muscle (Yang et al., 2020). Cis-chromatin interactions within TADs helps delineate enhancer-gene pairing and there is a remarkable similarity in chromosome looping between the cell and tissue-types (Rao et al., 2014), developmental stages (Yang et al., 2020) and even between species (Harmston et al., 2017; Kikuta et al., 2007). In both zebrafish brain and skeletal muscle, the first TAD at the end of chromosome 1, encompasses *runx1* and REN in a 1.28Mbp domain (Yang et al., 2020) suggesting they may interact (Fig. S4B). Activity by contact modeling of single-cell ATAC-sequencing from adult zebrafish brain (Yang et al., 2020) shows that REN and the *runx1* promoter are accessible within the same cells and therefore predicts REN is likely to be an enhancer of *runx1*.

In order to determine if REN regulates *runx1* in regenerating hearts, we measured changes in *runx1* mRNA in Δ*REN* mutants using droplet digital PCR (ddPCR) with a unique sensitivity where tens of thousands of PCR reactions are performed in parallel within separate lipid vesicles. The fraction of droplets that fluoresce from a successful PCR reaction are used to then extrapolate the original number of transcripts using the Poisson distribution. Using ddPCR we observed a 4.3-fold increase in the number of *runx1* transcripts during regeneration of wildtype hearts (Fig. 3G). Mutant Δ*REN* hearts, however, showed only a 2.4-fold increase or 57% of the wildtype during regeneration (Fig. 3G). The remaining increase in *runx1* abundance in Δ*REN* mutant hearts likely comes from endocardium, where the *runx1*-BAC reporter is induced (Koth et al., 2020) but *REN* regulates little to no expression (Fig. 1F). Therefore, we suggest that REN is an enhancer that regulates *runx1* expression in most cell types but not the endocardium. Interestingly, mRNA for *cbfb*, a binding partner and cofactor required for Runx1 transcriptional activity, increases during regeneration in our RNAseq of Δ*REN* mutant hearts (Fig. 3E, 5.2-fold, p-value 2.84×10^{-4}). Likely, a feedback loop is activated without *runx1* activation by *REN* during regeneration but not in uninjured hearts.

Previously, it was reported that *runx1* mutants, like Δ*REN* mutants, have increased CM proliferation during heart regeneration further supporting a role for *REN* enhancing *runx1* expression (Koth et al., 2020). One of the main conclusions of Koth et al. was that *runx1* mutants had differential composition of temporary scar within the clot after injury that they hypothesized is related to the CM proliferation changes (Koth et al., 2020). We do not observe similar changes in the abundance of collagen and fibrin in our Δ*REN* mutants. AFOG staining of Δ*REN* mutant hearts is indistinguishable from their wildtype siblings at either 3dpa (Fig. S5C) or 7dpa (Fig. S5D). We calculated fibrin and collagen within the scars using the described methodology and while we can detect expected differences between scarring at 3dpa and 7dpa, there are no differences between Δ*REN* mutants and their wildtype siblings (Fig. S5E, 3dpa chi-square p-value = 0.378, Fig. S5F, 7dpa chi-square p-value = 0.825). These data suggest that the observed differences in scarring in *runx1* mutants are unrelated to CM proliferation increases (please see Discussion for more details). Likely, *runx1* effects on CM proliferation are occurring in epicardium or myocardium where REN is controlling *runx1* expression.

REN expression around the outflow tract of uninjured hearts is inversely correlated to expression at the site of injury.

Expression of GFP in *REN:GFP* reporters is not unique to regeneration. In uninjured hearts, we observe GFP expression in CMs surrounding the valves leading from the ventricle to the outflow tract (Fig. 4A). Similar expression was observed in each of the three independent *REN* reporter lines that we originally generated (Goldman et al., 2017). As seen during regeneration, *REN:GFP* also expresses in non-CMs including in epicardial cells that emanate above the valve around the outflow tract (Fig. 4B). Calculation of relative GFP intensities showed that *REN:GFP* has 10X more GFP around uninjured valves as the rest of the uninjured ventricle (Fig. S4A) Interestingly, *REN:GFP* expression disappears in the myocardium surrounding the valve during regeneration with its nadir at 7dpa beginning to return by 14dpa and increasing to 21dpa (Fig. 4C-F). At 30dpa when most of the muscle has finished regrowing (Fig. 3A) REN:GFP expression reaches an equilibrium where it is on slightly less than half of its maximal expression in CM both around valves and in the freshly regrown site of injury (Fig. S4A). We conclude that peak of *REN* regulated gene expression is inversely correlated between CMs adjacent to valves and CMs that are undergoing regeneration. This suggests that REN activity is mechanistically connected in both expression domains.

To determine the minimal component of REN required for expression around valves, we looked at REN fragment reporter expression in uninjured hearts. REN fragments b12+ (Fig. S4B) and b1x (Fig. 4GH) both have activity in myocardium surrounding valves in uninjured hearts and the b2+ fragment does not (Fig. S4C). Thus, the 267bp minimal region of REN that is necessary and sufficient during regeneration is also necessary and sufficient for myocardial expression in uninjured hearts. We conclude that the same region of the genome is repurposed to activate genes in cardiac tissue, between uninjured valves and during regeneration.

Deletion of REN causes gene expression changes affecting outflow tract valves.

On occasion, reporters for transcriptional enhancers on occasion have subdomains of ectopic expression that do not reflect endogenous expression patterns (Bolt and Duboule, 2020). To confirm that the endogenous *REN* locus regulates genes in cardiac tissue adjacent to valves, we analyzed our RNAseq comparing Δ*REN* mutants and their wildtype siblings only looking at the uninjured replicates. There are 158 transcripts whose abundance significantly decreases by 75% and another 137 transcripts whose abundance significantly increases at least 3-fold in uninjured hearts of Δ*REN* mutants (Fig. 5A). The differential abundance of mRNA transcripts suggests that REN does indeed regulate gene expression *in vivo* in uninjured hearts. Likely, the majority of the transcripts with changing abundance are secondary effects of *REN* disruption and are not direct targets. Interestingly, gene ontology analysis of transcripts with increased abundance in Δ*REN* mutants included three members of the AP1 transcription factor complex, *fosab*, *fosb* and *atf3* each of which increase 26.3-fold, 11.62-fold and 9.08-fold respectively in uninjured mutant hearts (Fig. 5A, green dots). Therefore, disruption of *REN* resulted in increased levels of mRNAs encoding a transcription factor complex with motifs present in the deleted enhancer (Fig. S2A). This suggests that a feedback loop may be in place regulating *REN* activity in uninjured hearts.

The *REN:GFP* reporter shows that REN activates genes, suggesting that a direct target of REN *in vivo* would be among the transcripts that are less abundant in uninjured Δ*REN* mutant hearts. Of the 158 less abundant transcripts, 6 are encoded by genes found on chromosome 1 and none are found within the reported TAD with *REN* where most enhancer-promoter interactions lie (Sun et al., 2019; Symmons et al., 2014) (Fig. 5A). One gene, *adamts1*, was close. Only 672kb away from *REN, adamts1* sits just outside of the TAD towards the telomere and has been reported to interact with enhancers inside the REN containing TAD (Yang et al., 2020) (Fig.S5A). The *adamts1* gene encodes an extracellular matrix protein and regulates cardiac valves by degrading collagen (Hong-Brown et al., 2015). We note that we could not recapitulate the decrease in *adamts1* mRNA observed in our RNAseq experiment by ddPCR. To see if Δ*REN* mutants had observable phenotypes associated with Adamts1,

we stained Δ*REN* mutant hearts for collagen using AFOG and compared them to their wildtype siblings (Fig. 5BC, S5BC). Uninjured valves surrounding the outflow tract are visibly bluer in Δ*REN* mutant hearts indicating that they have more collagen. Taken together, deletion of endogenous *REN* results in decreased abundance of a cardiac valve associated gene *adamts1* by RNAseq with phenotypes in the valve associated with Adamts1 function.

From the *runx1*-BAC reporter, there is no detectable fluorescence in uninjured hearts (Koth et al., 2020) suggesting that *REN* expression in uninjured valves is distinct from *runx1* (Koth et al., 2020). There is also no detectable difference in *runx1* expression between uninjured wildtype and uninjured Δ*REN* mutant hearts (Fig. 3F) further suggesting that *REN* is regulating different gene(s) around the uninjured valves (Fig. 4). To determine if *REN* and *runx1* are in different pathways in uninjured hearts we performed a genetic complementation experiment (Fig. 5D). We crossed Δ*REN* heterozygotes to a *runx1* mutant line and compared compound heterozygotes containing one of each of the *REN* and *runx1* mutant alleles to their wildtype siblings. Uninjured hearts were stained for collagen by AFOG, and compound heterozygotes displayed similar levels of collagen as their wildtype siblings demonstrating that uninjured phenotypes in Δ*REN* mutant hearts do not depend on *runx1* (Fig. 5EF). Another gene is likely regulated by REN around valves that when dysregulated results in increases in collagen deposition.

Discussion

Here, we describe a transcriptional enhancer called REN that is active in cardiac tissue around the valve in uninjured hearts but is repurposed to activate at the site of injury during heart regeneration (Fig. 4). Targeted removal of this enhancer using CRISPR resulted in increased CM proliferation during regeneration and in increased collagen levels in valve leaflets in uninjured hearts (Fig. 3 and 5). Changes in underlying gene expression together with genetic complementation experiments show that different genes are regulated by REN during regeneration and in uninjured hearts (Fig. 5). Thus, rather than have a single enhancer co-regulating a group of genes, as it might do in other cell-types (Fig. S5A), REN likely regulates different genes temporally and in different subdomains within the heart. Interestingly, REN:GFP reporter expression was tied between these two domains, almost perfectly anti-correlated with one another up to 30 days into regeneration after muscle has regrown. Transcriptional enhancers for regeneration have been characterized to signal between organs during regeneration underlie evolution of regenerative capacity and used as tools to deliver pro-regenerative molecules in mammals (Sun et al., 2022; Wang et al., 2020; Yan et al., 2022; Zlatanova et al., 2023). However, mechanisms for how regenerative enhancers are recruited and targeted to critical genes are unknown. Here, we show that during regeneration, a particular enhancer can be repurposed from one function around cardiac valve to being recruited to activate a negative element in during heart regeneration and proliferation (Koth et al., 2020).

REN is very likely to directly regulate *runx1* during regeneration. Deletion of either gene or enhancer results in some very similar phenotypes; CM proliferation improves during regeneration (Koth et al., 2020). Single cell ATAC-seq from zebrafish brains uncovered an 'enhancer hub' where the promoters for *runx1* and genes for calcium channel homologs *atp1a1a.4*, *atp1a1a.3*, and *atp1a1a.5* all associate with REN (Fig. S5B)(James et al., 1999; Uyehara and Apostolou, 2023; Yang et al., 2020). This suggests that at least in the brain, REN forms a 'hub' to co-regulate these four genes across ~350Mbp. When REN is deleted, *runx1* expression is decreased during regeneration (Fig. 3F), confirming that also in the heart, REN regulates *runx1* expression at least in some cell-types. There must be additional enhancer(s) that govern *runx1* in endocardial cells during regeneration (Fig.1F) and *runx1* expression during hematopoietic development since Δ*REN* and *runx1*$^{\Delta TSS}$ double heterozygous mutants develop at Mendelian ratios unlike a *runx1* mutant homozygote (Koth et al., 2020; Lam et al., 2009; Sood et al., 2010).

Around cardiac valves in uninjured hearts, REN is unlikely to be regulating *runx1* because (1) unlike *REN*, *runx1* reporters do not express around cardiac valves (Koth et al., 2020), (2) *runx1* mRNA levels do not change in uninjured Δ*REN* mutant hearts (Fig. 3F), (3) runx1 co-regulator *cbfb* is only up-regulated in injured heart during regeneration in mutants and (4) most importantly, the *runx1* mutant allele compensates for Δ*REN* mutant phenotypes around valves (Fig. 5EF). We cannot exclude that valvular phenotypes do not result from misexpression of sodium potassium ion channels like the *atp1a1a* genes or another gene(s) within in the REN enhancer 'hub' (Fig. S5A)(James et al., 1999). Yet, we do not detect expression from the cluster of *atp1a1a* homologs and there are no active chromatin marks at the three *atp1a1a* promoters in zebrafish hearts (Goldman et al., 2017). REN likely regulates the *adamts1* gene either directly or indirectly since in uninjured Δ*REN* mutant hearts, valves have a phenotype consistent with decreased Adamts1 function (Santamaria and Groot, 2020) (Fig. 5BC). While *adamts1* does not sit in the same TAD as *runx1* in brain and muscle, there are interactions between promoters and enhancers from the end of chromosome 1 and promoters and enhancers within the *REN* containing TAD (Yang et al., 2020) (Fig. S5A). The *runx1* promoter interacts with an enhancer upstream of *adamts1* and the *adamts1* promoter interacts with an enhancer within the *REN*-containing TAD (Yang et al., 2020). This raises the possibility that *REN* could directly regulate *adamts1* across 672Mbp in cardiac tissue around valves in uninjured hearts.

Regeneration phenotypes for enhancers mutants are difficult to recover. There is a double requirement to have both a gene that when mutated would result in a phenotype *and* whose expression is dominated by a single enhancer. Here, we show that differences between enhancer mutants and gene mutants, reveal a clearer mechanistic understanding of gene function. In mutants for *runx1*, Koth et al. reported changes in clot composition in the wound during regeneration that is not observed in our REN mutants (Fig. S3C-F). This may be attributed to the fact that REN does not robustly activate in endocardial cells (Fig. 1F), a cell type that *runx1* is expressed in during heart regeneration and is at least partly responsible for scar deposition (Koth et al., 2020). Since Δ*REN* mutant hearts do not have differences in scar formation this strongly suggests that increases in CM proliferation in the *runx1* and Δ*REN* mutants are independent of observable differences in scarring.

Loss of function mutations that result in improved heart regeneration are not commonly described (Koth et al., 2020; Missinato et al., 2018). Why an anti-proliferative gene would be activated during regeneration is not obvious and poses a bit of a paradox. For example, at the peak of regeneration the REN enhancer is both a genetic marker of CM proliferation *and* activates an anti-proliferative program (Fig. 3) (Goldman et al., 2017). *A priori* one might expect that a program to slow regeneration would be temporally activated towards the conclusion of regeneration rather than the peak. We see no phenotypes in our Δ*REN* mutant hearts that would suggest regeneration is halted abnormally; however, we cannot exclude that there are redundancies regulating the end of regeneration. In mice, Runx1 is induced in certain models of dilated cardiomyopathy and knockout of *Runx1* in heart muscle improves recovery after heart injury (Kubin et al., 2011; McCarroll et al., 2018). However, changes in CM proliferation levels have not been described. Recently, *Runx1* has been reported to be linked to the abundance of more proliferative mono-nucleus diploid CMs (MNDCMs), which raises the possibility that expression of Runx1 in early stages of mouse post-natal development increase numbers of MNDCMs by preventing binucleation through inhibiting cytokinesis (González-Rosa et al., 2018; Patterson et al., 2017; Swift et al., 2023).

Acknowledgments

We would like to thank the American Heart Association for their support (GRANT #17SDG33660922 for JAG) and the Department of Biological Chemistry and Pharmacology, College of Medicine, Ohio State University Medical Center. The REN mutant strain and some REN fragment reporters were made in the Poss lab and we are grateful for his support and comments on this manuscript. Also, thanks to Arthur Burghes for access to the Droplet Digital PCR machine, loaning us Anton Blatnik, and manuscript comments.

Material and Methods

Transgenic fish construction – For reporter fish strains, the regulatory element being studied was cloned upstream of the mouse fos minimal promoter as previously described (Goldman et al., 2017). Stable transgenic zebrafish lines were produced using the I-Sce method of random genomic integration. The *tcf21*:Red reporter and the *flk*:Red reporters were previously published. All zebrafish (*Danio rerio*) used in this study derive from the Ekwill strain. Adults less than 1 year old were used for all the experiments. Males and females were mixed in similar proportions in each of the conditions. All experiments were performed under university supervision according to the institutional animal care and use committee protocol #2018R00000090 of Ohio State University.

Heart injuries – Zebrafish were anesthetized using Tricaine and placed ventral side up on a sponge to carry out resection of the ventricular apex. Iridectomy scissors were used to make an incision through the skin and pericardial sac. Gentle abdominal pressure exposed the heart and ~20% of the apex was removed with scissors, penetrating the chamber lumen (Poss et al., 2002). Hearts were harvested 1, 3, 7, 14, 21 or 30 days after injury depending on the experiment. To genetically ablate CMs, *cmlc2:CreER*^{pd10}*; bactin2:loxp-mCherry-STOP-loxp-DTA*^{pd36} (Z-CAT) fish were incubated in 0.5 μM tamoxifen for 17 h (Wang et al., 2011).

Immunofluorescence – Primary antibodies used in this study were: Rabbit anti-Mef2 (1:100, Abcam, ab197070), Rabbit anti-GFP (1:200, Life Technologies A11122) and Mouse anti-MF20 (1:100, Developmental Studies Hybridoma Bank, MF20). Secondary antibodies were: Goat anti-mouse Alexa Fluor 546 (1:200, Thermo Fisher Scientific, A-11030), and Goat anti-rabbit Alexa Fluor 488 (1:200, Thermo Fisher Scientific, A-11034).

Quantification of fluorescence

Average fluorescence – Briefly, using ImageJ, the red (or blue) channel was thresholded and used to select a region of interest in the green channel where the raw integrated density was calculated. Background was subtracted. The calculated fluorescence was then normalized to area under consideration.

CM proliferation - Injured fish were injected into the abdominal cavity once every 24 h for 3 days (4-6 dpa) with 10 μl of a 10 mM solution of EdU diluted in PBS. Hearts were removed on day 7, embedded and cryosectioned. Slides were stained with Alexa Fluor 594 Azide using click chemistry (Breinbauer and Köhn, 2003) and then immunostained for Mef2c. Briefly, sections were blocked with 1% bovine serum albumin (Fraction V) and 5% goat serum and washed in PBS with 0.2% Triton X-100. Three sections representing the largest wound area were selected from each heart and imaged using a 20× objective. The number of $Mef2^+$ and $Mef2^+EdU^+$ cells were counted using MIPAR image analysis software and the CM proliferation index was calculated as the number of $Mef2^+EdU^+$ cells/total $Mef2^+$ cells (Sosa et al., 2014). The CM proliferation index was averaged across two to four appropriate sections from each heart.

Mutant fish construction - Guide RNAs (sgRNAs) were designed against two regions flanking the REN element on chromosome 1 (sgUpstream: gTA gTg TTg Agg ATA gAC Ag, sgDownstream: gAA AAC AgC TAC AgC TCC CT). DNA templates of the respective sgRNA fused to a tracRNA were produced by PCR. T7-transcribed sgRNA were then injected with Cas9 protein into newly fertilized embryos from EK parents. Mutant strains were genotyped using PCR oligos (Fwd: gCC ACT gCC TCg CCC CTg Cg, Rev: AAT CgA TgA TTC TTg Agg TCA AAg ATg TgT ACT) for the mutant allele. A third oligo (ACA gCT ACA gCT CC TCg gAC) was added to the PCR to identify the wildtype allele. *REN* deletion was perfect without addition of extra nucleotides between the fused cut sites.

RNAseq analysis – Demultiplexed and quality-filtered reads, were aligned to the Danio rerio reference genome GRCz10 using Hierarchical Indexing for Spliced Alignment of Transcripts 2 (HISAT2) (Kim et al., 2015). Read counts for each gene were quantified using featureCounts software (Liao et al., 2014).

Differential gene expression analysis was performed using R package edgeR (McCarthy et al., 2012). The read counts were normalized using TMM method (Robinson and Oshlack, 2010). Differentially expressed genes were selected based on adjusted P value and log2 fold change.

Linear regression analysis - A master list of transcripts was created using the following criteria: (1) The transcript of interest had a P-value<0.05 for both the WT regeneration and Mut regeneration. (2) The transcript of interest had a $\log_2$FC>1 for either WT regeneration or Mut regeneration. Each transcript was assigned its WT regeneration $\log_2$FC as the X-value, and its Mut regeneration $\log_2$FC as the Y-value. A line of best fit was calculated using the master list, and residuals were calculated for each transcripts using the line of best fit. If its residual>1, then the transcript was colored red. If its residual<-1, then the transcript was colored blue.

AFOG staining – Acid Fushin Orange G staining was performed as previously described (Rao et al., 2023). For calculation of relative fibrin and collagen levels we adopted the methodology described in (Koth et al., 2020). Briefly, ImageJ was used to analyze the color of the wound area of sections stained with AFOG. Channels were split and images were color thresholded for red and blue using the same settings for all hearts. Red and blue particles were analyzed and %Area was recorded for each heart. To determine the orange area, %Red and %Blue values were subtracted from 100%. Percents were averaged from at least 5 hearts from each condition.

Statistics - To ensure that experiments were sufficiently powered we used an α error probability of 0.05 and 80% power to calculate if sample sizes were sufficient. For each analysis, we used the Welch's parametric *t*-test to calculate significance. If the variance between the comparison groups was also significant (*F* test for unequal variances), we switched to using a non-parametric test (Mann–Whitney). For the CM counting and CM proliferation assays, one researcher embedded hearts and sectioned slides and a separate researcher who was unaware of the sample identity carried out imaging and quantification.

Droplet-digital PCR - mRNA was isolated from wild-type and Δ*REN* uninjured and injured hearts using Trizol (Goldman et al., 2017). cDNA was made using 1µg RNA in Superscript II reverse transcriptase reactions incubated at 44 °C for 50 minutes. ddPCR assays were developed to detect *runx1*, *adamts1*, and *mob4* cDNA. cDNA for Mob4 served as loading control as it does not change in RNA-seq datasets in response to injury or between cell-types (REF Rao and from Rao). The primer and probe sequences for ddPCR are: *runx1* forward primer 5'-CgA gAg CCA CgA CgC CAC-3', *runx1* reverse primer 5'-CgA CTg CTC ATA CgA CCA ggA Tgg-3', runx1 probe 5'-/56-FAM/CAT gCg gTg/ZEN/ CAg CCC ACA CCA Cg/3IABkFQ/-3'; mob4 forward primer 5'- AgT ATT TTC CCA gCC gCg TCA gC -3', mob4 reverse primer 5'- TCA CgA AAC ggg TgA AgC gAT gAC -3', mob4 probe 5'-/HEX/TCC CAT gCg/ZEN/ TAC TTT CAC CAT CgC CAg/3IABkFQ/-3'; adamts1 forward primer 5'-gAg ACC TgC CCT gAT AGC AAT gg-3', adamts1 reverse primer 5'-ggT gTC CCA TCA gCC ACC T-3', adamts1 probe 5'-/56-FAM/CTG CAA gTT/ZEN/ ggT gTG CCg AgC gAA GG/3IABkFQ/-3'. We used 1 µL of reverse transcriptase reactions for detection of *runx1* and *adamts1* cDNA, and 1 µL of a 1:10 dilution of the cDNA was used to quantify *mob4*. Standard BioRad reaction conditions were used—10 µL 2x ddPCR Supermix for Probes (No dUTP) (cat# 1863023) 0.9 µM forward primer, 0.9 µM reverse primer, 0.25 µM probe, desired template amount and remaining volume of water to achieve 20 uL reaction volume. Reactions were partitioned into droplets using BioRad QX200 Droplet Generator (cat# 1864002), mixing 20 µL of reaction with 70 µL Droplet Generation Oil for Probes (cat#1863005). Droplets were transfered to Eppendorf 96-well twin.tec semi-skirted 96-well PCR Plates (cat# 951020389) and sealed with BioRad Pierceable Foil Heat Seal (cat# 1814040) using a Vitl Life Science Solutions Variable Temperature Sealer (cat# V902001). PCR thermocycling conditions were performed as follows: 50 °C for 2 minutes, 95°C for 2 minutes, 55 cycles of 95 °C 30 seconds, 60 °C for 1 minute, and 72 °C for 30 seconds, followed by 72 °C for 30 seconds, 12 °C forever, using BioRad T100 Thermal Cycler (cat# 1861096). Reactions were read using BioRad QX200 Droplet Reader (cat# 1864003) and thresholds were drawn

between the positive and negative droplet populations using the BioRad QX Software Version 2.1. Data was exported to Apple Numbers for further processing. Analysis of resulting data had to conform to >10,000 accepted reaction droplets, >1000 negative reaction droplets, and the number of positive droplets had to be greater than samples that did not receive reverse transcriptase. The calculated copies/µL for *runx1* and *adamts1* were normalized to *mob4*. These ratios were directly imported into GraphPad Prism to generate the figures.

Figure Legends

Figure 1. The REN enhancer expresses in epicardium and myocardium preceding the peak of regeneration.
(A) Myocardial expression of *REN:GFP* is shown by staining with Anti-MHC (blue) in hearts 7-days-post-amputation (dpa). (B) MIPAR rendition of colocalization in (A) shows colocalized regions in black and GFP that is not muscle positive in green. (C) Epicardial expression of *REN:GFP* is shown by colocalization with a *tcf21*:red (pink) reporter in hearts 7dpa. (D) MIPAR rendition of colocalization in (C) shows colocalized regions in black and GFP that is not *tcf21*-positive in green. (E) Endocardial expression of *REN:GFP* is shown by colocalization with a *flk*:red reporter in hearts 7dpa. (E') MIPAR rendition of flk colocalization from E is shown in black and *flk*-positive cells that are GFP-negative are shown in red. (F) Graph showing numbers of *flk*-positive/GFP-positive cells at 3dpa and 7dpa. (G) Graph showing the normalized GFP fluorescence of *REN:GFP* colocalized *tcf21*:Red (pink) and muscle (blue) at 3dpa and 7dpa. Zoom of muscle data is shown in the dashed box on the right.

Figure 2: Myocardial *REN*-directed gene expression is separable from other cell types.
(A) Cartoon represents a map of full-length REN (top green bar) and the seven smaller REN fragments that we tested in stable transgenic reporters. Fragments that induced GFP in epicardium are colored green and fragments that did not induce gene expression from a minimal promoter are colored gray. The epicardial specific region is outlined in a pink dashed box. (B-D) Left – Hearts from the one positive (B) REN-b12+ transgenic and the two negative (C) REN-b12 and (D) REN-b1x reporters at 3-days-post-amputation. Right – MIPAR renditions of colocalized areas are shown in black with excess GFP remaining in green. (E) Same cartoon as in (A) except fragments of REN are colored green based on their colocalization with cardiac muscle (stained with a myosin heavy chain (MHC) specific antibody) 7dpa. (F-H) Left - Hearts from the three positive reporter lines (F) REN-b12+, (G) REN-b12, and (H) REN-b1x Right – MIPAR renditions of colocalized areas are shown in black and white with excess GFP remaining in green.

Figure 3: Deletion of *REN* increases cardiomyocyte proliferation during regeneration. (A) Wildtype and mutant hearts were stained with MHC 30 days-after-amputation. (B) AFOG staining of the same hearts. (C) Images of sectioned amputated ventricles (7dpa) from wildtype and Δ*REN* mutant fish. Sections are stained for Mef2c (green) and EdU (red). Below – double positive cells are highlighted in black using a MIPAR software rendition (Scale bar = 100μm). (D) Quantification of CM proliferation indices (Mef2/EdU double positive over total Mef2 positive) in 7dpa ventricles (average WT = 9.11% and 11.71%; Mann-Whitney t-test, **p-value = 0.0094, N = 24 vs 19). Wildtype – blue, mutant – light blue. Horizontal black bars display the mean (middle) or standard error (top and bottom). (E) Scatterplot of RNAseq results comparing wildtype (x-axis) and Δ*REN* mutant (y-axis) samples. Each dot represents a transcript and are plotted by the $\log_2$ for the ratio of normalized reads from regeneration over normalized reads from the uninjured samples. Red dots are those transcripts that deviate by a linear regression >3-fold and blue dots are those transcripts that deviate by linear regression <-3-fold. Transcripts that are highlighted in the text are additionally marked in black circles. Green for pro-regeneration/proliferation genes, pink for sarcomeric genes, and runx1- coregulatory factor *cbfb*, dark red. (F) Venn diagram comparing chromatin marks at the promoters of genes whose mRNA either increases (left) or decreases (right) in Δ*REN* mutant hearts during regeneration. (G) Droplet Digital PCR shows the abundance of *runx1* transcripts increasing from uninjured wildtype hearts (blue) during heart regeneration (red) (average WT = 9.11% and 11.71%; Mann-Whitney t-test, **p-value = 0.0094, N = 24 vs 19). In Δ*REN* mutant fish (lighter colors), *runx1* levels increase less so (average WT = 9.11% and 11.71%; Mann-Whitney t-test, **p-value = 0.0094, N = 24 vs 19). Y-axis is the calculated *runx1* mRNA numbers normalized to calculated number of *mob4* mRNA.

Figure 4: *REN* regulates gene expression in cardiac tissue surrounding valves in uninjured hearts.

(A) Valves around the outflow tract in uninjured hearts are shown by endocardial reporter *flk*:Red (pink). REN:GFP (green) and muscle is stained with MHC (blue). (B) both cardiac muscle (MHC-blue) and epicardium (*tcf21* reporter, pink) colocalize with *REN:GFP* (green) around uninjured valves. (C-F) Same staining as in (A) but this time on regenerating hearts 3dpa (C), 7dpa (D), 14dpa (E), and 21dpa (F). Percentage of remaining GFP intensity is shown in the bottom left corner. (G) Quantification of average EGFP intensity in regions colocalizing with cardiac muscle (MHC). Cardiac valve regions are shown in blue and site of injury is shown in red. Y-axis is a timeline for the days after amputation of the ventricle apex.

Figure 5: *REN* regulates different genes in uninjured hearts and during regeneration.

(A) Volcano plot showing differences in RNAseq from uninjured wildtype hearts vs uninjured Δ*REN* hearts. Transcripts of genes decreasing within 1.7Mb of REN on chromosome 1 are highlighted in pink and labeled with arrows. Members of the AP1 transcription factor complex are highlighted in green and labeled with arrows. (B-C) AFOG staining of uninjured wildtype (B) and uninjured Δ*REN* mutant hearts (C). Region around the outflow tract valve is shown with a zoom of the valve leaflets on the right. (D) Cartoon of complementation experiment. Shown are the regions of chromosome 1 deleted in the Δ*REN* and Δ*runx1* mutant lines (dashed blue boxes). The Y-axis is the enrichment of cardiomyocyte specific–histone H3.3 and the X-axis are coordinates along chromosome 1. (E-F) AFOG staining of uninjured wildtype (E) and uninjured Δ*REN* / Δ*runx1* double heterozygote hearts (F). Region around the outflow tract valve is shown with a zoom of the valve leaflets on the right.

Supplemental Figure Legends

Supp Figure 1 –
(A) Time course of *REN:GFP* expression throughout the heart during regeneration. REN – green, MHC – blue. (B) Quantification of total area containing GFP fluorescence.

Supp Figure 2 –
(A) Cartoon of REN with example Cardiomyocyte Regeneration Motifs (CRM) shown from each of the four blocks. (B-E) Heart sections from the different REN fragments (labeled) in ZCAT hearts ablated 7 days-post-induction. Left – gray scale of GFP. Right – MHC (red), REN:GFP (green).

Supp Figure 3 -
(A) Diagram of the Δ*REN* deletion mutant showing site of chromosome breakage and the 9 nucleotides inserted during the repair. (B) Quantification of CM proliferation indices (Mef2/EdU double positive over total Mef2 positive) in uninjured ventricles (wildtype average = 0.78%; mutant average = 0.54%; Welch's t-test, p-value = .252, N = 7 vs 11). Wildtype – blue, mutant – light blue. Horizontal black bars display the mean (middle) or standard error (top and bottom). (C) Graph of total Mef2-positive CM numbers counts in adult uninjured hearts (average = 2095 and 1666; Welch's t-test, p-value = 0.115, N = 7 vs 11). (D) Cartoon of the TAD containing both *REN* and *runx1* in adult zebrafish brain and muscle. (E-F) Representative image of injury site from wildtype and Δ*REN* mutant hearts stained with AFOG at 3 days-post-amputation (E) and 7dpa (F). (G) Calculation of relative fibrin (red) and collagen (blue) levels from 3dpa based on Koth et al. methodology. wildtype averages: collagen = 7.75%; fibrin = 8.70%; muscle (orange) = 83.73%; mutant averages: collagen = 5.16%; fibrin = 12.60%; muscle (orange) = 82.25%; Chi-square p-value = 0.3376; N=7,5. (H) Calculation of relative fibrin (red) and collagen (blue) levels from 7dpa based on Koth et al. methodology. wildtype averages: collagen = 1.13%; fibrin = 5.36%; muscle (orange) = 93.51%; mutant averages: collagen = 1.35%; fibrin = 3.89%; muscle (orange) = 93.51%; Chi-square p-value = 0.825; N=5,6.

Supp Figure 4 –
(A) Minimal fragment of REN is sufficient for CM expression around uninjured valves (REN-b1X); muscle (blue) and GFP (green). Right - MIPAR rendition of colocalized areas from REN-b1X are shown in black with excess GFP remaining in green. (B) REN fragments b12+ (C) and b2+.

Supp Figure 5 –
(A) Cartoon of the entire region of chromosome 1 including the telomeric end and the TAD containing both *REN* and *runx1*. Genes are shown as arrows with dotted lines representing 3D interactions found by Hi-ChIP. The loop marked 1 is the interaction of the *adamts1* promoter with an enhancer within the TAD. The loop marked 2 is the interaction between the *runx1* and an enhancer outside of the TAD nearby *adamts1*. (B) Cartoon showing the 'REN enhancer hub' where promoters for *runx1* and the three *atp1a1a* genes all interact with one another and with REN. (C-D) AFOG staining of uninjured wildtype (C) and uninjured Δ*REN* mutant hearts (D). Images are zoomed in on the region around valves near the outflow tract. All replicates are included here to show consistency of the result in Figure 5BC.

References

Abascal, F., Acosta, R., Addleman, N. J., Adrian, J., Afzal, V., Ai, R., Aken, B., Akiyama, J. A., Jammal, O. A., Amrhein, H., et al. (2020). Expanded encyclopaedias of DNA elements in the human and mouse genomes. *Nature* **583**, 699–710.

Bahr, C., Paleske, L. von, Uslu, V. V., Remeseiro, S., Takayama, N., Ng, S. W., Murison, A., Langenfeld, K., Petretich, M., Scognamiglio, R., et al. (2018). A Myc enhancer cluster regulates normal and leukaemic haematopoietic stem cell hierarchies. *Nature* **553**, 1 27.

Beisaw, A., Kuenne, C., Guenther, S., Dallmann, J., Wu, C.-C., Bentsen, M., Looso, M. and Stainier, D. Y. R. (2020). AP-1 Contributes to Chromatin Accessibility to Promote Sarcomere Disassembly and Cardiomyocyte Protrusion During Zebrafish Heart Regeneration. *Circ Res* **126**, 1760–1778.

Bolt, C. C. and Duboule, D. (2020). The regulatory landscapes of developmental genes. *Development* **147**, dev171736.

Cao, Y., Xia, Y., Balowski, J. J., Ou, J., Song, L., Safi, A., Curtis, T., Crawford, G. E., Poss, K. D. and Cao, J. (2022). Identification of enhancer regulatory elements that direct epicardial gene expression during zebrafish heart regeneration. *Development* **149**,.

Cho, S. W., Xu, J., Sun, R., Mumbach, M. R., Carter, A. C., Chen, Y. G., Yost, K. E., Kim, J., He, J., Nevins, S. A., et al. (2018). Promoter of lncRNA Gene PVT1 Is a Tumor- Suppressor DNA Boundary Element. *Cell* **173**, 1398 1400.e22.

Cuellar-Partida, G., Buske, F. A., McLeay, R. C., Whitington, T., Noble, W. S. and Bailey, T. L. (2012). Epigenetic priors for identifying active transcription factor binding sites. *Bioinformatics* **28**, 56–62.

Dao, L. T. M., Galindo-Albarrán, A. O., Castro-Mondragon, J. A., Andrieu-Soler, C., Medina-Rivera, A., Souaid, C., Charbonnier, G., Griffon, A., Vanhille, L., Stephen, T., et al. (2017). Genome-wide characterization of mammalian promoters with distal enhancer functions. *Nat. Genet.* **49**, 1073–1081.

Fanucchi, S., Shibayama, Y., Burd, S., Weinberg, M. S. and Mhlanga, M. M. (2013). Chromosomal contact permits transcription between coregulated genes. *Cell* **155**, 606 620.

Fukaya, T., Lim, B. and Levine, M. (2016). Enhancer Control of Transcriptional Bursting. *Cell* **166**, 358–368.

Fulco, C. P., Munschauer, M., Anyoha, R., Munson, G., Grossman, S. R., Perez, E. M., Kane, M., Cleary, B., Lander, E. S. and Engreitz, J. M. (2016). Systematic mapping of functional enhancer–promoter connections with CRISPR interference. *Science* **354**, 769–773.

Gasperini, M., Hill, A. J., McFaline-Figueroa, J. L., Martin, B., Kim, S., Zhang, M. D., Jackson, D., Leith, A., Schreiber, J., Noble, W. S., et al. (2019). A Genome-wide Framework for Mapping Gene Regulation via Cellular Genetic Screens. *Cell* **176**, 377-390.e19.

Goldman, J. A., Kuzu, G., Lee, N., Karasik, J., Gemberling, M., Foglia, M. J., Karra, R., Dickson, A. L., Sun, F., Tolstorukov, M. Y., et al. (2017). Resolving Heart Regeneration by Replacement Histone Profiling. *Dev Cell* **40**, 392 404.e5.

González-Rosa, J. M., Sharpe, M., Field, D., Soonpaa, M. H., Field, L. J., Burns, C. E. and Burns, C. G. (2018). Myocardial Polyploidization Creates a Barrier to Heart Regeneration in Zebrafish. *Dev Cell* **44**, 433 446.e7.

Harmston, N., Ing-Simmons, E., Tan, G., Perry, M., Merkenschlager, M. and Lenhard, B. (2017). Topologically associating domains are ancient features that coincide with Metazoan clusters of extreme noncoding conservation. *Nat. Commun.* **8**, 441.

Hnisz, D., Shrinivas, K., Young, R. A., Chakraborty, A. K. and Sharp, P. A. (2017). A Phase Separation Model for Transcriptional Control. *Cell* **169**, 13 23.

Hong□Brown, L. Q., Brown, Cr., Navaratnarajah, M. and Lang, C. H. (2015). Adamts1 Mediates Ethanol□Induced Alterations in Collagen and Elastin via a FoxO1□Sestrin3□AMPK Signaling Cascade in Myocytes. *J. Cell. Biochem.* **116**, 91–101.

James, P. F., Grupp, I. L., Grupp, G., Woo, A. L., Askew, G. R., Croyle, M. L., Walsh, R. A. and Lingrel, J. B. (1999). Identification of a Specific Role for the Na,K-ATPase α2 Isoform as a Regulator of Calcium in the Heart. *Mol. Cell* **3**, 555–563.

Jopling, C., Sleep, E., Raya, M., Martí, M., Raya, A. and Belmonte, J. C. I. (2010). Zebrafish heart regeneration occurs by cardiomyocyte dedifferentiation and proliferation. *Nature* **464**, 606 609.

Kang, J., Hu, J., Karra, R., Dickson, A. L., Tornini, V. A., Nachtrab, G., Gemberling, M., Goldman, J. A., Black, B. L. and Poss, K. D. (2016). Modulation of tissue repair by regeneration enhancer elements. *Nature* **532**, 201 206.

Kikuchi, K. and Poss, K. D. (2012). Cardiac regenerative capacity and mechanisms. *Annu Rev Cell Dev Bi* **28**, 719 741.

Kikuchi, K., Holdway, J. E., Werdich, A. A., Anderson, R. M., Fang, Y., Egnaczyk, G. F., Evans, T., Macrae, C. A., Stainier, D. Y. R. and Poss, K. D. (2010). Primary contribution to zebrafish heart regeneration by gata4(+) cardiomyocytes. *Nature* **464**, 601 605.

Kikuchi, K., Holdway, J. E., Major, R. J., Blum, N., Dahn, R. D., Begemann, G. and Poss, K. D. (2011a). Retinoic acid production by endocardium and epicardium is an injury response essential for zebrafish heart regeneration. *Dev Cell* **20**, 397 404.

Kikuchi, K., Gupta, V., Wang, J., Holdway, J. E., Wills, A. A., Fang, Y. and Poss, K. D. (2011b). tcf21+ epicardial cells adopt non-myocardial fates during zebrafish heart development and regeneration. *Development* **138**, 2895 2902.

Kikuta, H., Laplante, M., Navratilova, P., Komisarczuk, A. Z., Engström, P. G., Fredman, D., Akalin, A., Caccamo, M., Sealy, I., Howe, K., et al. (2007). Genomic regulatory blocks encompass multiple neighboring genes and maintain conserved synteny in vertebrates. *Genome Res.* **17**, 545–555.

Kim, D., Langmead, B. and Salzberg, S. L. (2015). HISAT: a fast spliced aligner with low memory requirements. *Nat. Methods* **12**, 357–360.

Koth, J., Wang, X., Killen, A. C., Stockdale, W. T., Potts, H. G., Jefferson, A., Bonkhofer, F., Riley, P. R., Patient, R. K., Göttgens, B., et al. (2020). Runx1 promotes scar deposition and inhibits myocardial proliferation and survival during zebrafish heart regeneration. *Development* **147**, dev186569.

Kubin, T., Pöling, J., Kostin, S., Gajawada, P., Hein, S., Rees, W., Wietelmann, A., Tanaka, M., Lörchner, H., Schimanski, S., et al. (2011). Oncostatin m is a major mediator of cardiomyocyte dedifferentiation and remodeling. *Cell Stem Cell* **9**, 420 432.

Kvon, E. Z., Waymack, R., Gad, M. and Wunderlich, Z. (2021). Enhancer redundancy in development and disease. *Nat Rev Genet* **22**, 324–336.

Lam, E. Y. N., Chau, J. Y. M., Kalev-Zylinska, M. L., Fountaine, T. M., Mead, R. S., Hall, C. J., Crosier, P. S., Crosier, K. E. and Flores, M. V. (2009). Zebrafish runx1 promoter-EGFP transgenics mark discrete sites of definitive blood progenitors. *Blood* **113**, 1241 1249.

Lee, H. J., Hou, Y., Chen, Y., Dailey, Z. Z., Riddihough, A., Jang, H. S., Wang, T. and Johnson, S. L. (2020). Regenerating zebrafish fin epigenome is characterized by stable lineage-specific DNA methylation and dynamic chromatin accessibility. *Genome Biol* **21**, 52.

Liao, Y., Smyth, G. K. and Shi, W. (2014). featureCounts: an efficient general purpose program for assigning sequence reads to genomic features. *Bioinformatics* **30**, 923–930.

Lim, B., Heist, T., Levine, M. and Fukaya, T. (2018). Visualization of Transvection in Living Drosophila Embryos. *Mol. Cell* **70**, 287-296.e6.

Lowe, V., Wisniewski, L., Sayers, J., Evans, I., Frankel, P., Mercader-Huber, N., Zachary, I. C. and Pellet-Many, C. (2019). Neuropilin 1 mediates epicardial activation and revascularization in the regenerating zebrafish heart. *Development* **146**, dev174482 13.

Lowe, V., Wisniewski, L. and Pellet-Many, C. (2021). The Zebrafish Cardiac Endothelial Cell—Roles in Development and Regeneration. *J. Cardiovasc. Dev. Dis.* **8**, 49.

Lupiáñez, D. G., Kraft, K., Heinrich, V., Krawitz, P., Brancati, F., Klopocki, E., Horn, D., Kayserili, H., Opitz, J. M., Laxova, R., et al. (2015). Disruptions of Topological Chromatin Domains Cause Pathogenic Rewiring of Gene-Enhancer Interactions. *Cell* **161**, 1012–1025.

Mahmoud, A. I., Kocabas, F., Muralidhar, S. A., Kimura, W., Koura, A. S., Thet, S., Porrello, E. R. and Sadek, H. A. (2013). Meis1 regulates postnatal cardiomyocyte cell cycle arrest. *Nature* **497**, 249 253.

Markenscoff-Papadimitriou, E., Allen, W. E., Colquitt, B. M., Goh, T., Murphy, K. K., Monahan, K., Mosley, C. P., Ahituv, N. and Lomvardas, S. (2014). Enhancer interaction networks as a means for singular olfactory receptor expression. *Cell* **159**, 543 557.

McCarroll, C. S., He, W., Foote, K., Bradley, A., Mcglynn, K., Vidler, F., Nixon, C., Nather, K., Fattah, C., Riddell, A., et al. (2018). Runx1 Deficiency Protects Against Adverse Cardiac Remodeling After Myocardial Infarction. *Circulation* **137**, 57–70.

McCarthy, D. J., Chen, Y. and Smyth, G. K. (2012). Differential expression analysis of multifactor RNA-Seq experiments with respect to biological variation. *Nucleic Acids Res.* **40**, 4288–4297.

Melo, U. S., Schöpflin, R., Acuna-Hidalgo, R., Mensah, M. A., Fischer-Zirnsak, B., Holtgrewe, M., Klever, M.-K., Türkmen, S., Heinrich, V., Pluym, I. D., et al. (2020). Hi-C Identifies Complex Genomic Rearrangements and TAD-Shuffling in Developmental Diseases. *Am. J. Hum. Genet.* **106**, 872–884.

Miguel-Escalada, I., Bonàs-Guarch, S., Cebola, I., Ponsa-Cobas, J., Mendieta-Esteban, J., Atla, G., Javierre, B. M., Rolando, D. M. Y., Farabella, I., Morgan, C. C., et al. (2019). Human pancreatic islet

three-dimensional chromatin architecture provides insights into the genetics of type 2 diabetes. *Nat Genet* **51**, 1137–1148.

Missinato, M. A., Saydmohammed, M., Zuppo, D. A., Rao, K. S., Opie, G. W., Kühn, B. and Tsang, M. (2018). Dusp6 attenuates Ras/MAPK signaling to limit zebrafish heart regeneration. *Development* **145**, dev157206.

Nameki, R. A., Chang, H., Yu, P., Abbasi, F., Lin, X., Reddy, J., Haro, M., Fonseca, M. A., Freedman, M. L., Drapkin, R., et al. (2023). Rewiring of master transcription factor cistromes during high-grade serous ovarian cancer development.

Oegema, K., Savoian, M. S., Mitchison, T. J. and Field, C. M. (2000). Functional Analysis of a Human Homologue of the Drosophila Actin Binding Protein Anillin Suggests a Role in Cytokinesis. *J. Cell Biol.* **150**, 539–552.

Okada, H. and Saga, Y. (2022). Repurposing of the enhancer-promoter communication underlies the compensation of Mesp2 by Mesp1. *PLoS Genet.* **18**, e1010000.

Oudelaar, A. M., Harrold, C. L., Hanssen, L. L. P., Telenius, J. M., Higgs, D. R. and Hughes, J. R. (2019). A revised model for promoter competition based on multi-way chromatin interactions at the α-globin locus. *Nat. Commun.* **10**, 5412.

Panigrahi, A. and O'Malley, B. W. (2021). Mechanisms of enhancer action: the known and the unknown. *Genome Biol.* **22**, 108.

Patterson, M., Barske, L., Handel, B. V., Rau, C. D., Gan, P., Sharma, A., Parikh, S., Denholtz, M., Huang, Y., Yamaguchi, Y., et al. (2017). Frequency of mononuclear diploid cardiomyocytes underlies natural variation in heart regeneration. *Nat Genet* **49**, 1346 1353.

Pelham-Webb, B., Murphy, D. and Apostolou, E. (2020). Dynamic 3D Chromatin Reorganization during Establishment and Maintenance of Pluripotency. *Stem Cell Rep.* **15**, 1176–1195.

Poss, K. D., Wilson, L. G. and Keating, M. T. (2002). Heart regeneration in zebrafish. *Science* **298**, 2188 2190.

Rao, S. S. P., Huntley, M. H., Durand, N. C., Stamenova, E. K., Bochkov, I. D., Robinson, J. T., Sanborn, A. L., Machol, I., Omer, A. D., Lander, E. S., et al. (2014). A 3D Map of the Human Genome at Kilobase Resolution Reveals Principles of Chromatin Looping. *Cell* **159**, 1665–1680.

Rao, A., Lyu, B., Jahan, I., Lubertozzi, A., Zhou, G., Tedeschi, F., Jankowsky, E., Kang, J., Carstens, B., Poss, K., et al. (2023). The translation initiation factor homolog, eif4e1c, regulates cardiomyocyte metabolism and proliferation during heart regeneration. *Development* **150**, dev201376.

Robinson, M. D. and Oshlack, A. (2010). A scaling normalization method for differential expression analysis of RNA-seq data. *Genome Biol.* **11**, R25–R25.

Sabari, B. R., Dall'Agnese, A., Boija, A., Klein, I. A., Coffey, E. L., Shrinivas, K., Abraham, B. J., Hannett, N. M., Zamudio, A. V., Manteiga, J. C., et al. (2018). Coactivator condensation at super-enhancers links phase separation and gene control. *Science* **361**, eaar3958 13.

Santamaria, S. and Groot, R. de (2020). ADAMTS proteases in cardiovascular physiology and disease. *Open Biol.* **10**, 200333.

Sood, R., English, M. A., Belele, C. L., Jin, H., Bishop, K., Haskins, R., McKinney, M. C., Chahal, J., Weinstein, B. M., Wen, Z., et al. (2010). Development of multilineage adult hematopoiesis in the zebrafish with a runx1 truncation mutation. *Blood* **115**, 2806 2809.

Sosa, J. M., Huber, D. E., Welk, B. and Fraser, H. L. (2014). Development and application of MIPAR^{TM}: a novel software package for two- and three-dimensional microstructural characterization. *Integrating Mater Manuf Innovation* **3**, 123–140.

Sun, F., Chronis, C., Kronenberg, M., Chen, X.-F., Su, T., Lay, F. D., Plath, K., Kurdistani, S. K. and Carey, M. F. (2019). Promoter-Enhancer Communication Occurs Primarily within Insulated Neighborhoods. *Mol. Cell* **73**, 250-263.e5.

Sun, F., Ou, J., Shoffner, A. R., Luan, Y., Yang, H., Song, L., Safi, A., Cao, J., Yue, F., Crawford, G. E., et al. (2022). Enhancer selection dictates gene expression responses in remote organs during tissue regeneration. *Nat Cell Biol* **24**, 685–696.

Swift, S. K., Purdy, A. L., Kolell, M. E., Andresen, K. G., Lahue, C., Buddell, T., Akins, K. A., Rau, C. D., O'Meara, C. C. and Patterson, M. (2023). Cardiomyocyte ploidy is dynamic during postnatal development and varies across genetic backgrounds. *Development* **150**,.

Symmons, O., Uslu, V. V., Tsujimura, T., Ruf, S., Nassari, S., Schwarzer, W., Ettwiller, L. and Spitz, F. (2014). Functional and topological characteristics of mammalian regulatory domains. *Genome Res.* **24**, 390–400.

Takayama, Y., Kamimura, Y., Okawa, M., Muramatsu, S., Sugino, A. and Araki, H. (2003). GINS, a novel multiprotein complex required for chromosomal DNA replication in budding yeast. *Genes Dev.* **17**, 1153–1165.

Thompson, J. D., Ou, J., Lee, N., Shin, K., Cigliola, V., Song, L., Crawford, G. E., Kang, J. and Poss, K. D. (2020). Identification and requirements of enhancers that direct gene expression during zebrafish fin regeneration. *Development* **147**, dev191262.

Uyehara, C. M. and Apostolou, E. (2023). 3D enhancer-promoter interactions and multi-connected hubs: Organizational principles and functional roles. *Cell Rep.* **42**, 112068.

Wang, Y., Kaiser, M. S., Larson, J. D., Nasevicius, A., Clark, K. J., Wadman, S. A., Roberg-Perez, S. E., Ekker, S. C., Hackett, P. B., McGrail, M., et al. (2010). Moesin1 and Ve-cadherin are required in endothelial cells during in vivo tubulogenesis. *Development* **137**, 3119–3128.

Wang, J., Panáková, D., Kikuchi, K., Holdway, J. E., Gemberling, M., Burris, J. S., Singh, S. P., Dickson, A. L., Lin, Y.-F., Sabeh, M. K., et al. (2011). The regenerative capacity of zebrafish reverses cardiac failure caused by genetic cardiomyocyte depletion. *Development* **138**, 3421 3430.

Wang, J., Cao, J., Dickson, A. L. and Poss, K. D. (2015). Epicardial regeneration is guided by cardiac outflow tract and Hedgehog signalling. *Nature* **522**, 226 230.

Wang, W., Hu, C.-K., Zeng, A., Alegre, D., Hu, D., Gotting, K., Granillo, A. O., Wang, Y., Robb, S., Schnittker, R., et al. (2020). Changes in regeneration-responsive enhancers shape regenerative capacities in vertebrates. *Science* **369**, eaaz3090.

Wei, K., Serpooshan, V., Hurtado, C., Diez-Cuñado, M., Zhao, M., Maruyama, S., Zhu, W., Fajardo, G., Noseda, M., Nakamura, K., et al. (2015). Epicardial FSTL1 reconstitution regenerates the adult mammalian heart. *Nature* **525**, 479 485.

Wilber, A., Nienhuis, A. W. and Persons, D. A. (2011). Transcriptional regulation of fetal to adult hemoglobin switching: new therapeutic opportunities. *Blood* **117**, 3945–3953.

Yan, R., Cigliola, V., Oonk, K. A., Petrover, Z., DeLuca, S., Wolfson, D. W., Vekstein, A., Mendiola, M. A., Devlin, G., Bishawi, M., et al. (2022). An enhancer-based gene-therapy strategy for spatiotemporal control of cargoes during tissue repair. *Cell Stem Cell* **30**, 96-111.e6.

Yang, H., Luan, Y., Liu, T., Lee, H. J., Fang, L., Wang, Y., Wang, X., Zhang, B., Jin, Q., Ang, K. C., et al. (2020). A map of cis-regulatory elements and 3D genome structures in zebrafish. *Nature* 1–7.

Youngblood, M. W., Erson-Omay, Z., Li, C., Najem, H., Co□kun, S., Tyrtova, E., Montejo, J. D., Miyagishima, D. F., Barak, T., Nishimura, S., et al. (2023). Super-enhancer hijacking drives ectopic expression of hedgehog pathway ligands in meningiomas. *Nat. Commun.* **14**, 6279.

Zlatanova, I., Sun, F., Wu, R. S., Chen, X., Lau, B. H., Colombier, P., Sinha, T., Celona, B., Xu, S.-M., Materna, S. C., et al. (2023). An injury-responsive mmp14b enhancer is required for heart regeneration. *Sci. Adv.* **9**, eadh5313.

Figure 1

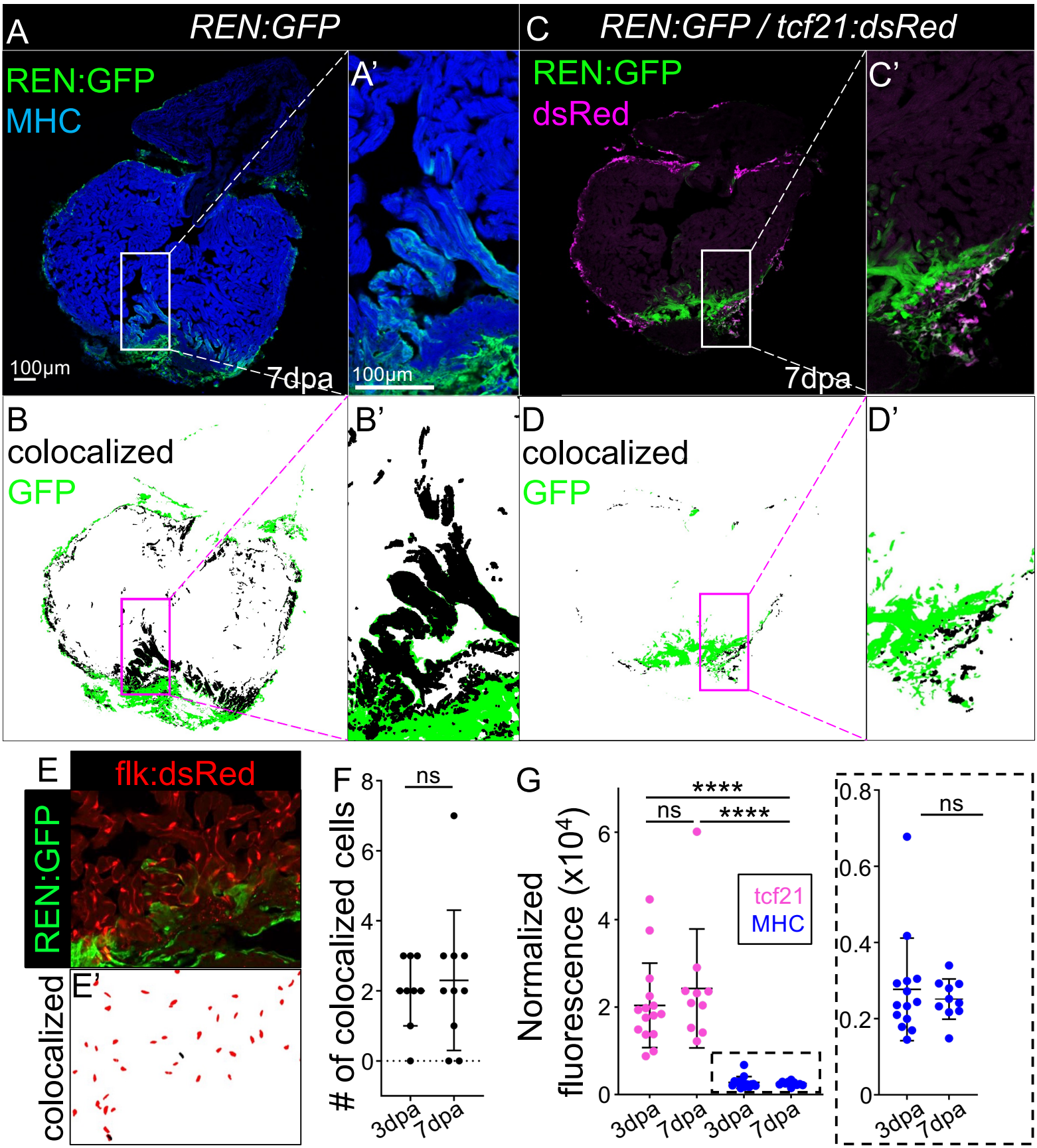
A
REN:GFP
REN:GFP
MHC
100µm
7dpa
A'
100µm
C
REN:GFP / tcf21:dsRed
REN:GFP
dsRed
7dpa
C'
B
colocalized
GFP
B'
D
colocalized
GFP
D'
E
flk:dsRed
REN:GFP
E'
colocalized
F
# of colocalized cells
ns
3dpa
7dpa
G
Normalized fluorescence (x10^4)
****
ns
****
tcf21
MHC
3dpa
7dpa
3dpa
7dpa
ns
3dpa
7dpa

Figure 2

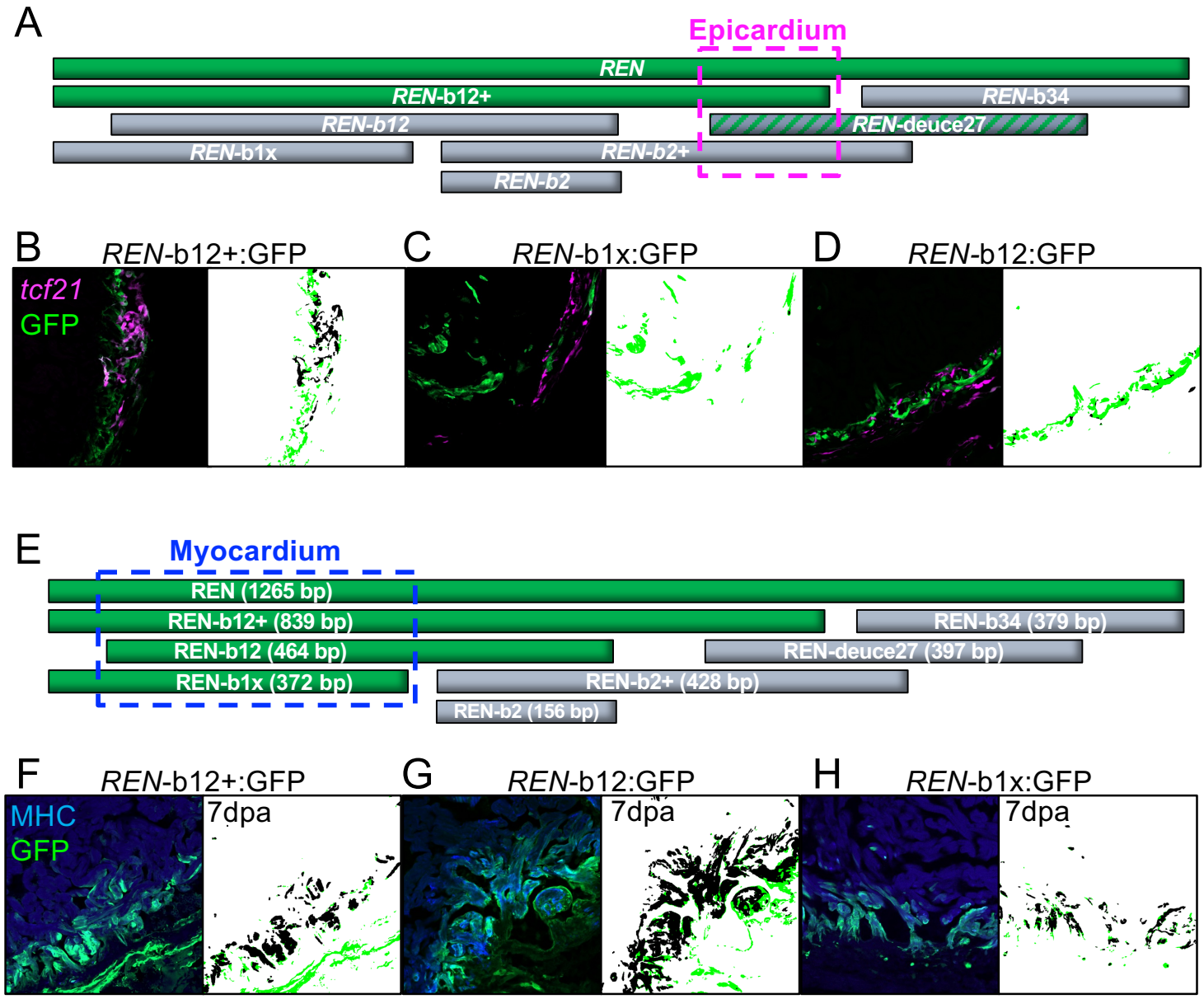
A
Epicardium
REN
REN-b12+
REN-b34
REN-b12
REN-deuce27
REN-b1x
REN-b2+
REN-b2
B
REN-b12+:GFP
tcf21
GFP
C
REN-b1x:GFP
D
REN-b12:GFP
E
Myocardium
REN (1265 bp)
REN-b12+ (839 bp)
REN-b34 (379 bp)
REN-b12 (464 bp)
REN-deuce27 (397 bp)
REN-b1x (372 bp)
REN-b2+ (428 bp)
REN-b2 (156 bp)
F
REN-b12+:GFP
MHC
GFP
7dpa
G
REN-b12:GFP
7dpa
H
REN-b1x:GFP
7dpa

Figure 3

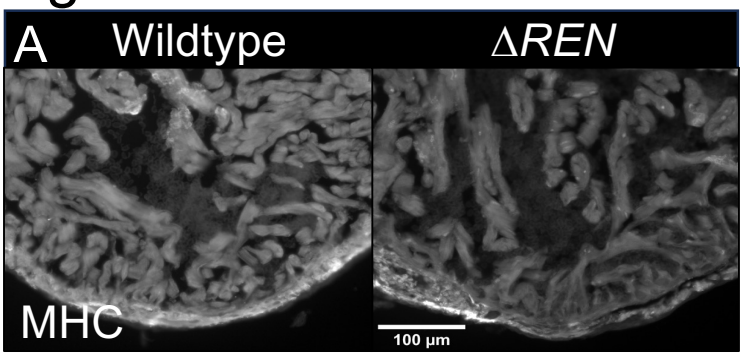
A
Wildtype
ΔREN
MHC
100 µm

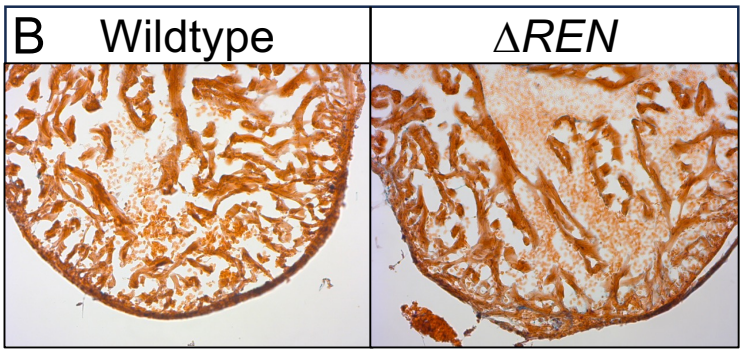
B
Wildtype
ΔREN

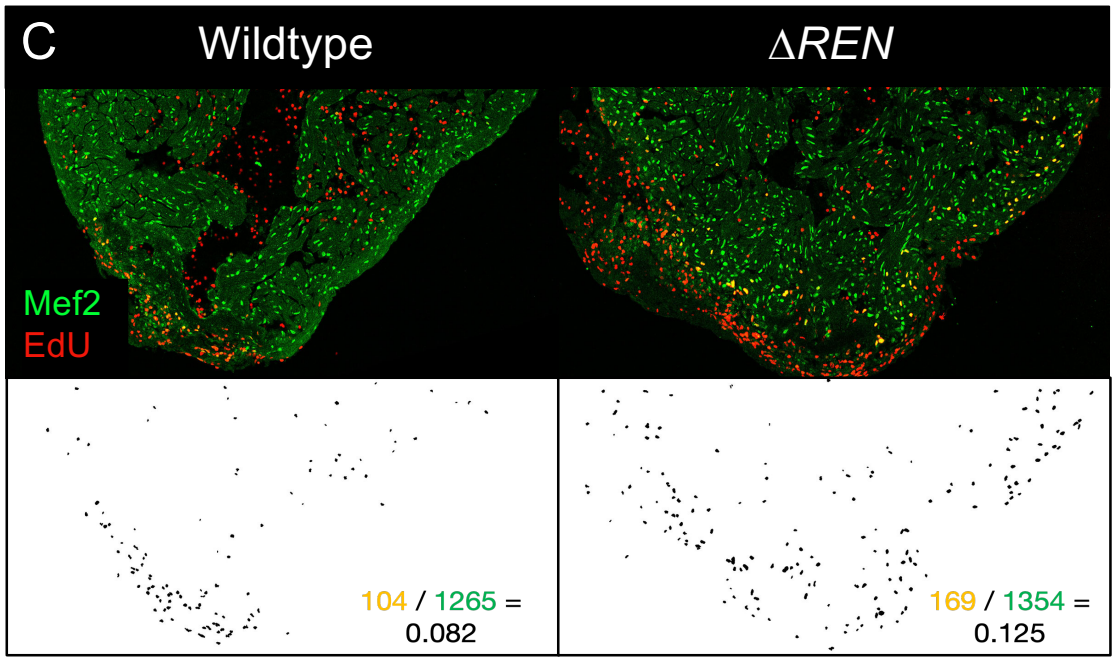
C
Wildtype
ΔREN
Mef2
EdU
104 / 1265 =
0.082
169 / 1354 =
0.125

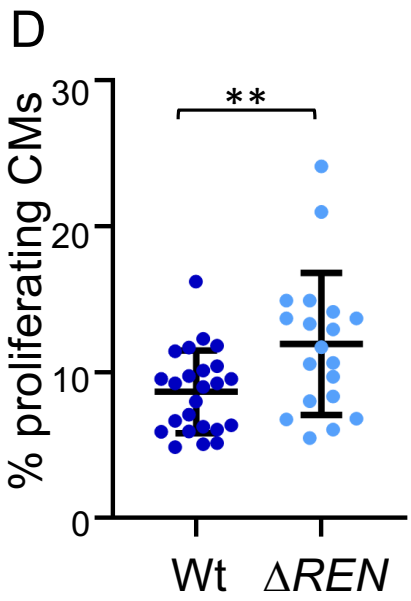
D
% proliferating CMs
30
20
10
0
**
Wt
ΔREN

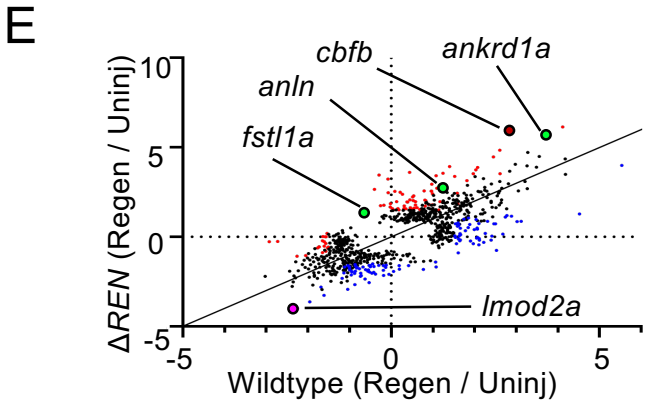
E
ΔREN (Regen / Uninj)
Wildtype (Regen / Uninj)
cbfb
ankrd1a
anln
fstl1a
lmod2a
10
5
0
-5
-5
0
5

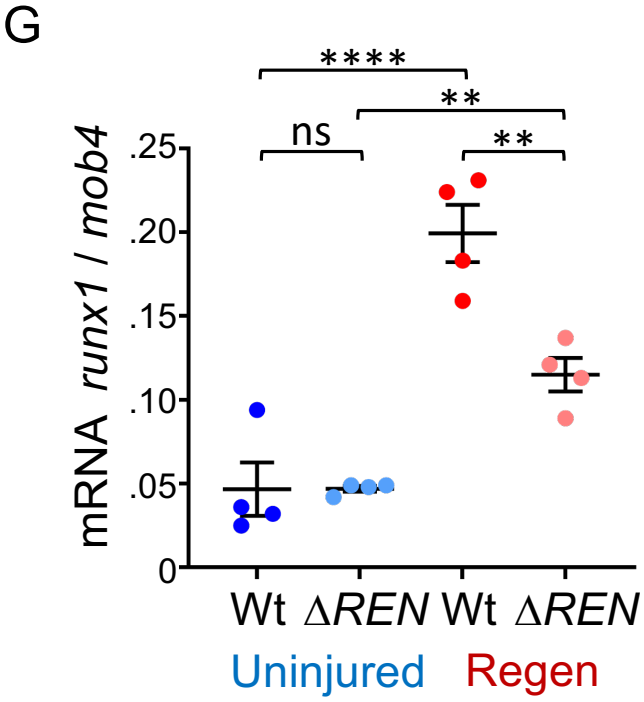
G
mRNA runx1 / mob4
.25
.20
.15
.10
.05
0
****
**
ns
**
Wt
ΔREN
Wt
ΔREN
Uninjured
Regen

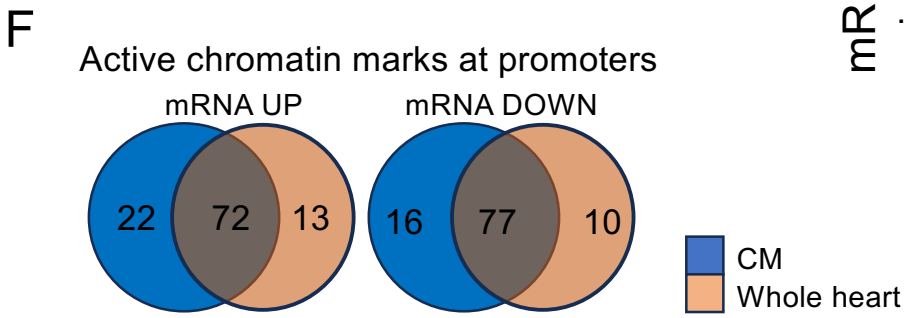
F
Active chromatin marks at promoters
mRNA UP
mRNA DOWN
22
72
13
16
77
10
CM
Whole heart

Figure 4

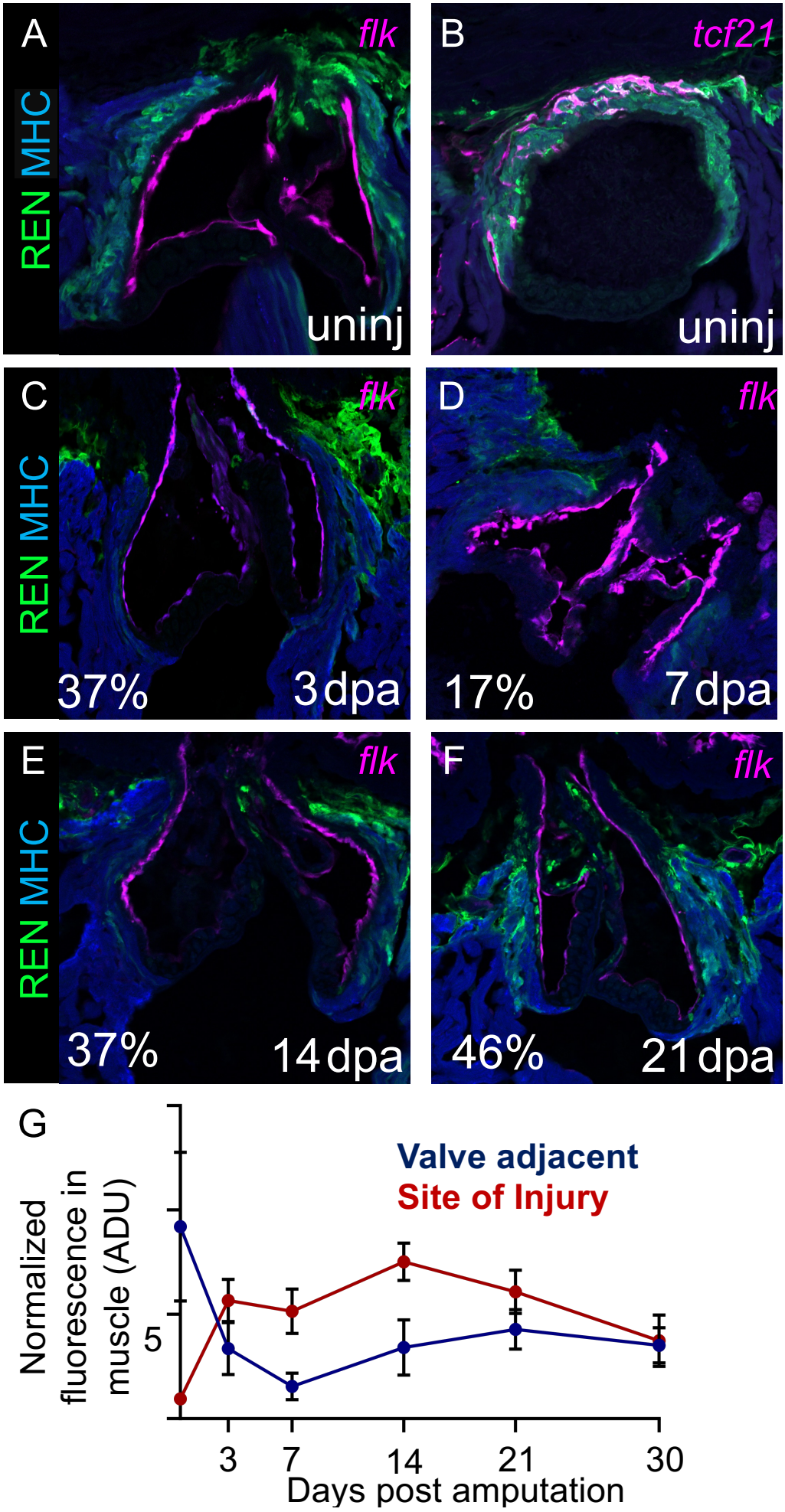
A
flk
REN MHC
uninj
B
tcf21
uninj
C
flk
REN MHC
37%
3 dpa
D
flk
17%
7 dpa
E
flk
REN MHC
37%
14 dpa
F
flk
46%
21 dpa
G
Valve adjacent
Site of Injury
Normalized fluorescence in muscle (ADU)
5
3
7
14
21
30
Days post amputation

Figure 5

A

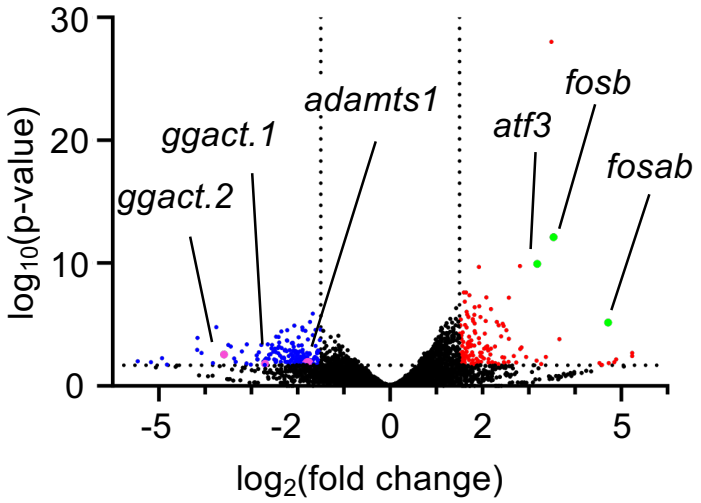
30
20
10
0
-5
-2
0
2
5
log10(p-value)
log2(fold change)
ggact.2
ggact.1
adamts1
atf3
fosb
fosab

D

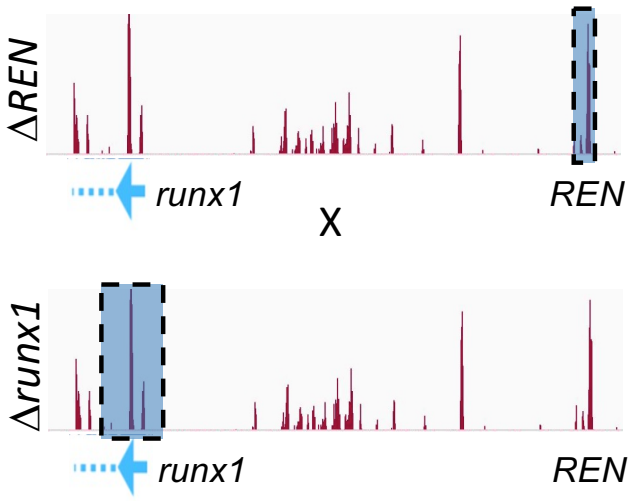
ΔREN
runx1
REN
X
Δrunx1
runx1
REN

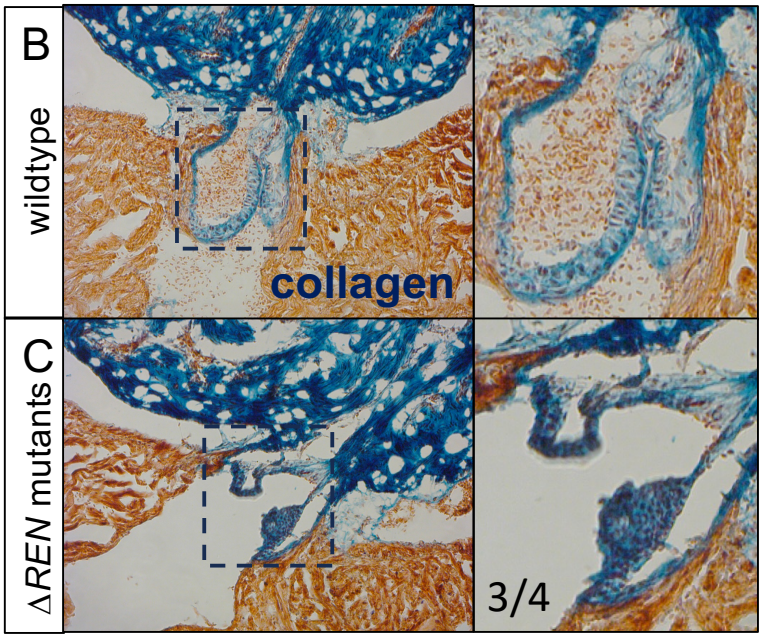
B
wildtype
collagen
C
ΔREN mutants
3/4

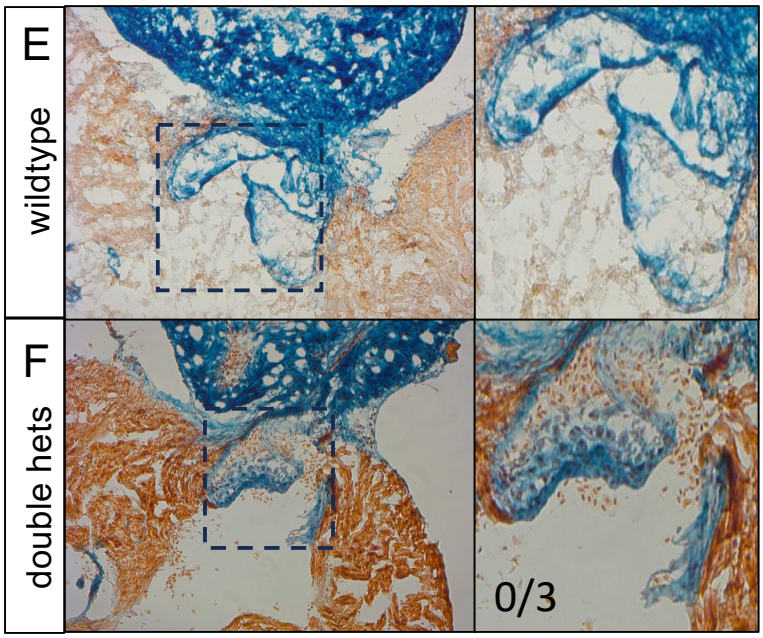
E
wildtype
F
double hets
0/3